Bioorganic Chemistry 169 (2026) 109376

Contents lists available at ScienceDirect

Bioorganic Chemistry

journal homepage: www.elsevier.com/locate/bioorg

Self-assembled nanoparticles of glycosylated AABB-type phthalocyanines for selective photodynamic therapy

Irene Paramio [a], Gaole Dai [b], Tomás Torres [a,c,d,*], Dennis K.P. Ng [b,*], Gema de la Torre [a,c,*]

[a] Universidad Autónoma de Madrid, C/ Francisco Tomás y Valiente 7, 28049, Madrid, Spain
[b] Department of Chemistry, The Chinese University of Hong Kong, Shatin, N.T., Hong Kong, China
[c] Institute for Advanced Research in Chemical Sciences (IAdChem). Universidad Autónoma de Madrid, 28049, Madrid, Spain
[d] Instituto Madrileño de Estudios Avanzados (IMDEA)-Nanociencia, C/ Faraday 9, Csantoblanco, 28049 Madrid, Spain

ARTICLE INFO

Keywords:
Photodynamic therapy
Phthalocyanines
Amphiphiles
Self-assembly
Nanoparticles
Glucose transporters

ABSTRACT

Photodynamic therapy (PDT) is still hindered by limitations such as poor bioavailability and insufficient selectivity towards tumor cells. To overcome these drawbacks, nanostructured delivery systems have emerged as promising platforms due to their ability to enhance bioavailability and achieve efficient tumor targeting. In this context, nanoparticles (NPs) formed by the self-assembly of highly amphiphilic photosensitizers (PS) in aqueous media are particularly attractive. Among the various PS available, phthalocyanines (Pcs) are especially suitable for constructing nanoassemblies for PDT owing to their outstanding optical and photophysical properties, as well as their ability to form stable nanoaggregates in water through a combination of π–π stacking and hydrophobic interactions. In this work, we describe the design, synthesis, and evaluation of two amphiphilic, glucose-functionalized zinc(II) phthalocyanines (Zn(*II*)Pcs) as self-assembled PS for PDT. These derivatives are obtained from binaphthyloxy-linked AABB-type Zn(*II*)Pc synthons previously reported by our group, which are functionalized at the binaphthol ring with glucose units via Sonogashira coupling or copper-catalyzed click reaction. The resulting amphiphiles, **GluPc-1** and **GluPc-2**, spontaneously self-assemble into stable NPs (15–30 nm) that undergo partial disassembly inside cells, which restores the photophysical properties required for efficient PDT. Notably, the glucose moieties exposed on the NP surface enhance selective uptake by tumor cells overexpressing glucose transporters (GLUT-1). Biological studies in cancerous (A549 and HT29) and non-cancerous (HEK293) cell lines confirmed preferential uptake in GLUT1-positive cells, while cytotoxicity assays demonstrated negligible dark toxicity and potent light-induced phototoxic effects.

1. Introduction

Photodynamic therapy (PDT) is considered an effective and benign alternative to other traditional treatments for early-stage cancers [1]. It involves two individually non-toxic components: a photosensitizer (PS) and light of specific wavelength in the phototherapeutic window (600–850 nm). PS are innocuous in the dark, but after photoirradiation, they can be activated to a triplet excited state, which subsequently transfers its energy to molecular oxygen, generating singlet oxygen ($^1O_2$) and other reactive oxygen species (ROS) [2]. These reactions occur in the immediate vicinity of the light-absorbing PS; therefore, PDT is highly spatiotemporal selective. However, PDT is still not adopted as a regular cancer treatment due to suboptimal outcomes derived from low uptake and non-selective accumulation in malignant tissues. Recently, the development of nanostructured delivery systems has led to enhanced therapeutic effects by improving bioavailability and tumor targeting efficacy by means of the enhanced permeability and retention (EPR) effect [3]. In this regard, the use of nanoparticles (NPs) obtained by self-assembly in aqueous solutions of PS with strong amphiphilic character deserves special attention [4–6], because they may address the limitations concerning the multistep fabrication and low reagent loadings of traditional polymeric or inorganic nanostructured delivery systems.

Within the extended PS collection, phthalocyanines (Pcs) and in particular Zn(*II*)Pcs are targets of choice to build nanoassemblies for PDT, due to their outstanding optical and photophysical properties: high quantum yield of $^1O_2$ generation, low dark toxicity and chemical stability [7,8]. Adequate functionalization of Pcs with hydrophilic chains leads to customized amphiphilic systems that can spontaneously

* Corresponding authors.
E-mail addresses: tomas.torres@uam.es (T. Torres), dkpn@cuhk.edu.hk (D.K.P. Ng), gema.delatorre@uam.es (G. de la Torre).

https://doi.org/10.1016/j.bioorg.2025.109376
Received 7 October 2025; Received in revised form 25 November 2025; Accepted 11 December 2025
Available online 18 December 2025
0045-2068/© 2025 The Authors. Published by Elsevier Inc. This is an open access article under the CC BY-NC license (http://creativecommons.org/licenses/by-nc/4.0/).

assemble in aqueous solution. For these extended π-conjugated molecules, hydrophobic and *π-π* interactions are the main noncovalent interactions driving the assembly [9], although modulating hydrophilic substitution can help counterbalance the attractive interactions between hydrophobic regions. Therefore, a careful structural design may render NPs forming stable dispersions with uniform nanosized distribution but showing some degree of disassembly in the cellular interior that enables recovery of the photophysical properties, which are usually cancelled in the aggregates. Aiming at preparing highly directional amphiphilic Zn(*II*)Pcs, we have recently followed a synthetic approach consisting in the cross-condensation of binaphthyloxy-linked bisphthalonitriles and non-functionalized single phthalonitriles to obtain molecules with an AABB substitution pattern in good yields [10]. AABB-type Pcs represent a structurally intriguing class of compounds, but difficult to prepare by conventional statistical methods based on the cross-condensation of two differently substituted phthalonitrile precursors [11,12]. Despite these synthetic limitations, AABB Pcs are highly valuable synthons for the preparation of Pc-based amphiphiles, since the controlled arrangement of substituents among the isoindole units enables the introduction of well-defined amphiphilic properties. In this context, the use of pre-linked bisphthalonitrile intermediates can effectively guide the cross-condensation reaction with a second phthalonitrile precursor, facilitating the selective formation of AABB-type Pcs. The rigid chiral binaphthol scaffold plays a key role in promoting the successful synthesis of these asymmetrically substituted Pcs, in contrast to more flexible linkers, which tend to favor the formation of oligomeric byproducts [13,14]. Furthermore, amphiphilic chains can be conveniently introduced at the binaphthol core, enabling straightforward access to the desired amphiphilic derivatives. Finally, the intrinsic chirality of the binaphthol unit may induce the formation of chiral supramolecular nanostructures, allowing the self-assembly process to be monitored by circular dichroism (CD) spectroscopy. Another particular aspect of these Pcs is that the supramolecular organization in aqueous media is also governed by steric hindrance imposed by the rigid binaphthol core, which has an influence on the growth and stability of the NPs. Following this strategy, several cationic AABB Zn(*II*)Pcs have been reported, showing efficient antibacterial PDT behavior due to improved interactions of the positively charged NPs with negatively charged outer membrane of bacteria [15–17].

In this work, we describe the preparation of amphiphilic glucose-functionalized AABB Zn(*II*)Pcs, designed to promote their self-assembly in aqueous media into stable NPs. It is envisioned that these nanostructured PS will show increased cellular uptake in tumoral cells due to a multivalent effect towards glucose transporters that are over-expressed in a wide range of cancer cells. Moreover, we expect that the presence of the binaphthol may contribute to weaken to some extent the strong π-π interactions between Pc molecules, facilitating some degree of disassembly in the cellular interior which leads to the recovery of the photophysical activity which is lost in the extracellular NPs. Two different compounds, **GluPc-1** and **GluPc-2** were designed to study a possible influence of the linkage between the Zn(*II*)Pc chromophores and the glucose moieties in the self-assembly behavior (Fig. 1). Both compounds could be prepared using highly efficient synthetic procedures, namely Sonogashira coupling for **GluPc-1**, and copper-catalyzed azide-alkyne cycloaddition (CuAAC) "click reaction" for **GluPc-2**. As a result, the latter would incorporate a 1,2,3-triazole linker, which could have a role on the self-assembly process due to the presence of coordinative *N*-centred lone-pairs.

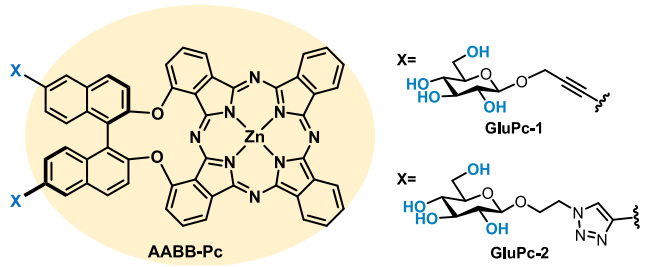

Fig. 1. Chemical structure of **GluPc-1** and **GluPc-2.**

2. Results and discussion

2.1. Synthesis

The synthetic routes towards **GluPc-1** and **GluPc-2** are shown in Scheme 1. The strategic AABB Zn(*II*)Pc synthons (**AABB-Br** [10], **AABB-alk** [10,16] and **AABB-alkH** [16]) have been prepared following our previously described procedures.

For the synthesis of **GluPc-1** (Scheme 1a), two different approaches were followed. In first place, **AABB-Br** [10] was prepared in 21% yield by mixed condensation of binapthol-bisphthalonitrile **AA-Br** and phthalonitrile following the conditions optimized by our group. Subsequent coupling with commercially available 2-propynyl-tetra-*O*-acetyl-β-D-glucopyranoside (**Glu-1**) was performed using copper-free Sonogashira conditions, which had proved efficient with related substrates, yielding **GluAABB-1** in 34%. This low-to-moderate yield led us to try an alternative approach which entailed performing the coupling reaction over the bisphthalonitrile precursor **AA-Br** under the same copper-free conditions. In this case, pure **AA-Glu** bisphthalonitrile was isolated in high yield (89%). Next, we attempted the mixed condensation of **AA-Glu** with the non-functionalized phthalonitrile **B**, but the reaction rendered compound **GluAABB-1** in only 10% yield. Therefore, the two routes resulted in a similar overall yield. The final step was the alkaline hydrolysis to remove the acetate protecting groups from the glucose to obtain **GluPc-1**. The ^{1}H NMR spectrum of the compound (see characterization in SI) showed the disappearance of the signals corresponding to the acetate protons (2.00–1.80 ppm), and the upfield shift of the signal of the C—H protons of the carbohydrate compared to the acetylated precursor. Corresponding changes were observed by ^{13}C NMR spectral analysis. Additionally, in the ^{1}H NMR spectrum of **GluPc-1** in DMSO-d_6, the proton signals corresponding to each alcohol group of the glucose moiety were clearly identified by a COSY experiment (see Fig. 2). The structure was further confirmed by HR-MS analysis.

Turning to **GluPc-2**, it was synthesized via CuAAC click reaction between the acetylene containing Zn(*II*)Pc synthon **AABB-alkH** [16] and the modified glucose derivative **Glu-2** containing an azide moiety [18]. The reaction was performed using $CuSO_4{\cdot}5H_2O$ with sodium ascorbate in catalytic amounts in a mixture of THF/H_2O as solvent, giving **GluAABB-2** in 60% yield. Deprotection of the carbohydrates under alkaline conditions yielded **GluPc-2**, which was fully characterized by ^{1}H NMR (see Fig. 2), ^{13}C NMR and HR-MS.

2.2. Photophysical and aggregation studies

Initially, ground-state absorption spectra of **GluPc-1** and **GluPc-2** were recorded in DMSO, in which both compounds were molecularly dissolved. Results are summarized in Table 1. The spectra displayed the typical Q-band and B-band transitions expected for non-aggregated species, with Q-band maxima at 680 nm, and B-band maxima at 350 and 351 nm for **GluPc-1** and **GluPc-2**, respectively. Both derivatives exhibited good fluorescence emission, with maxima at 687 nm and 688 nm, and fluorescence quantum yields (Φ_F) of 0.14 and 0.16, respectively. Moreover, the monomeric forms showed high singlet oxygen generation efficiencies, with quantum yields (Φ_Δ) of 0.62 and 0.61 for **GluPc-1** and **GluPc-2**, respectively.

The high directional amphiphilic character of **GluPc-1** and **GluPc-2** is expected to promote self-assembly in aqueous media, as previously observed for related structures [15–17]. Therefore, their aggregation behavior was investigated using UV–vis and fluorescence spectroscopy. Although neither of the two carbohydrate-substituted Pcs proved

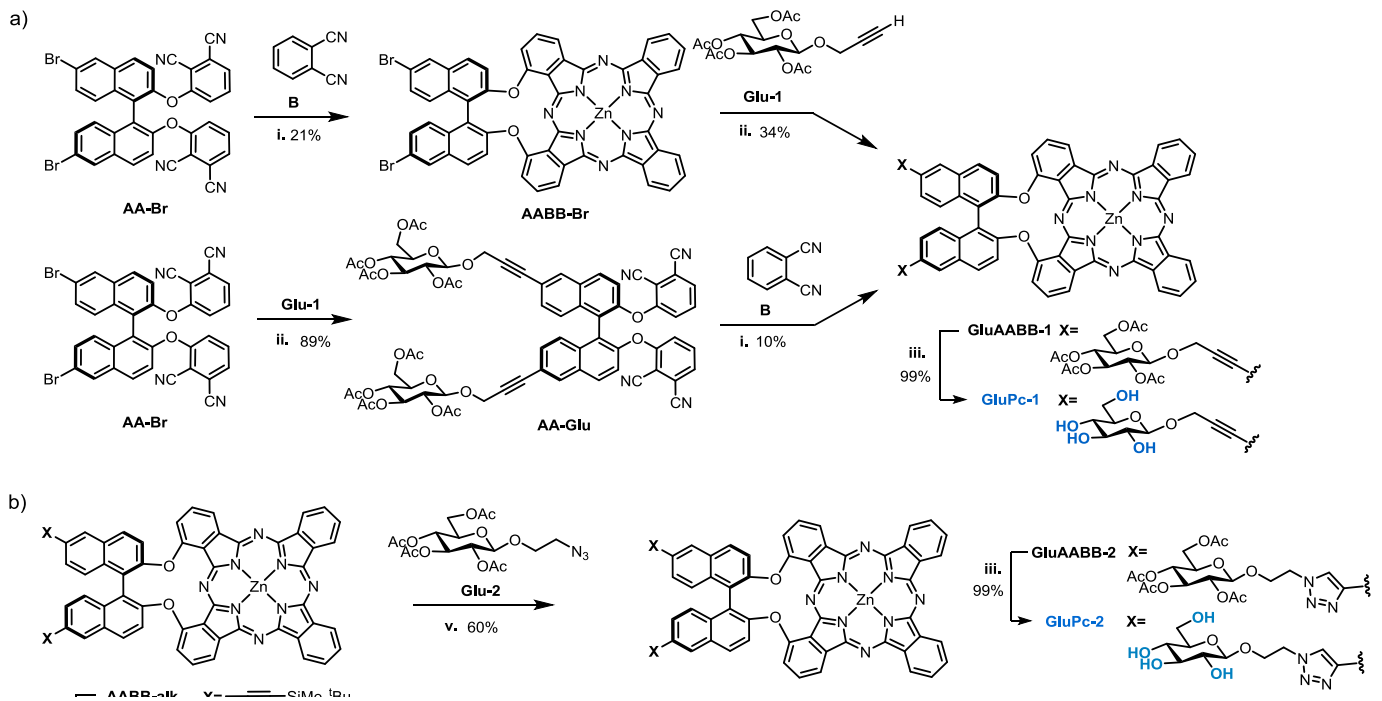

Scheme 1. Synthetic routes towards a) **GluPc-1** and b) **GluPc-2**. i. $Zn(OAc)_2$, *o*-DCB/DMF 2:1 at 150 °C for 16 h; ii. $Pd(PPh_3)_4$ in DMF/Et_3N 2:1, 80 °C; iii. Na(s) in DMSO/MeOH 2:1 at rt.; vi. TBAF in THF, 0 °C to rt. for 2 h; v. $CuSO_4{\cdot}5H_2O$ and sodium ascorbate in THF/H_2O 3:1, rt. for 16 h.

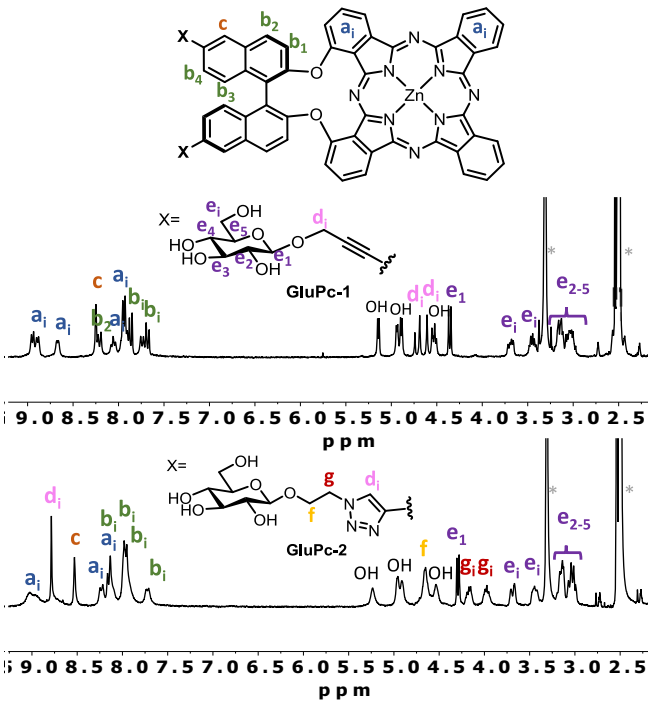

Fig. 2. ^{1}H NMR spectra of **GluPc-1** (top) and **GluPc-2** (bottom) in DMSO-d_6.

soluble in pure water, both of them remained soluble in 99:1 H_2O/DMSO solutions. Therefore, aggregation studies were carried out by measuring solutions at different H_2O/DMSO ratios while keeping the concentration constant (Fig. 3a and b). Starting from dilute DMSO solutions, progressive addition of water led to a decrease in Q-band intensity, accompanied by the emergence of a new band at lower

Table 1
Photophysical properties of **GluPc-1** and **GluPc-2** in DMSO and H_2O.

Compound	Solvent	logε (λ)	λ_f[b] / nm	Φ_F[c]	Φ_Δ[d]
GluPc-1	DMSO	4.7 (350) 4.4 (612) 5.2 (680)	687	0.14	0.62
	H_2O[a]	4.5 (335) 4.5 (633) 4.4 (684)	–	<<0.001	–
GluPc-2	DMSO	4.7 (351) 4.5 (613) 5.3 (680)	688	0.16	0.61
	H_2O[a]	4.6 (337) 4.5 (634) 4.4 (679)	–	<<0.001	–

[a] Samples in H_2O/DMSO 99:1, prepared from DMSO stock solutions.
[b] λ_{exc}: 650 nm.
[c] λ_{exc}: 630 nm.
[d] Measured in DMSO using the singlet oxygen quencher 1,3-diphenylisobenzofuran (DPBF).

wavelength (633 and 634 nm for **GluPc-1** and **GluPc-2**, respectively, in 99% H_2O). This observation, together with the drop in fluorescence intensity (Φ_F<<0.001 in 99% H_2O), suggests the formation of *H*-type aggregates. Specifically, both Q-band absorption and fluorescence intensity decreased sharply between 20% and 50% H_2O content. Interestingly, **GluPc-2** exhibited an additional feature in the UV–vis spectra; between 50% and 70% water content, a new absorption band appeared at longer wavelengths (796 nm), reaching a maximum at 70%, and disappearing upon further increasing the water content to 80%. This red-shifted band is consistent with the formation of *J*-type aggregates under these conditions [19,20], which possibly originates from the presence of the coordinating triazole ring which promotes a slipped cofacial arrangement of the stacked rings through coordination to the Zn (*II*) centre [21–23]. However, upon increasing the water content (from 80% on), the hydrophobic forces rule the aggregation behavior, minimizing other directional forces.

To deepen in the self-assembly behavior of **GluPc-2**, a denaturation study of the aggregate in the 70% H_2O solution was carried out by

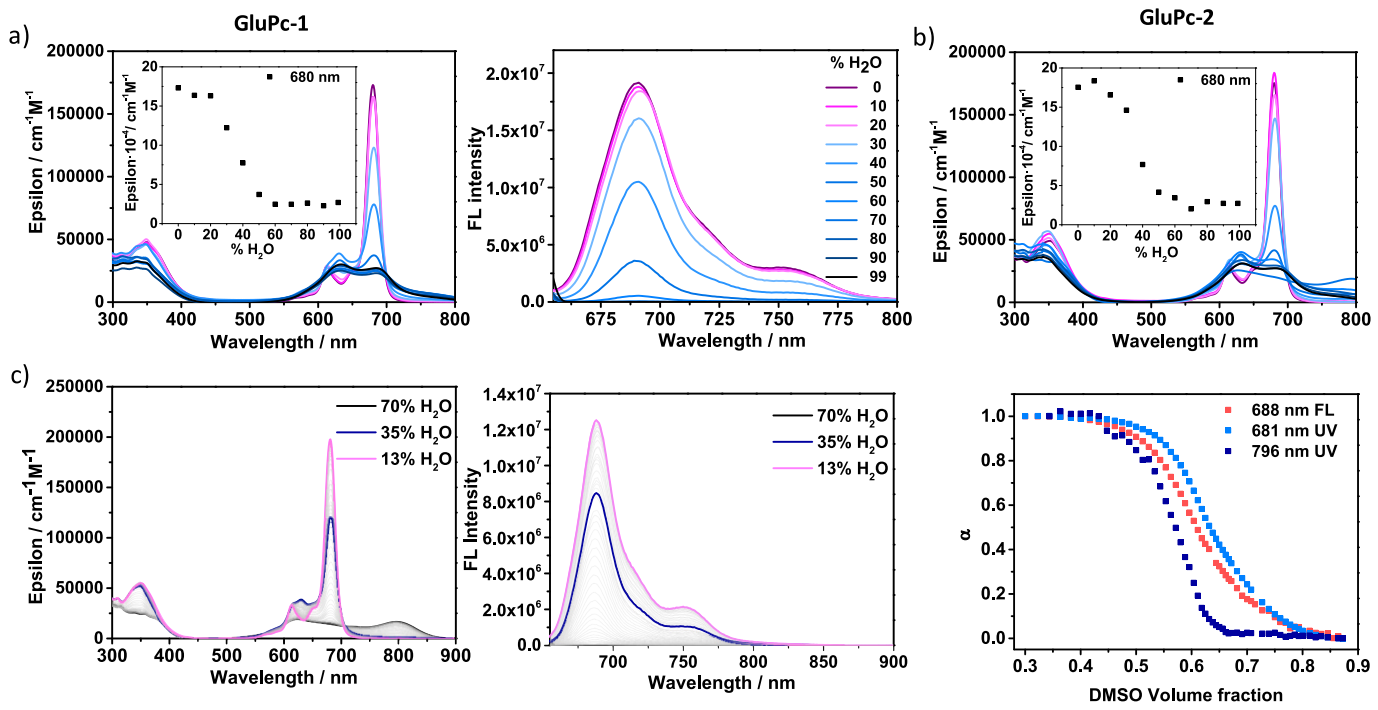

Fig. 3. Absorption and emission solvent-dependent studies of a) **GluPc-1** ($5{\cdot}10^{-6}$ M) and b) absorption of **GluPc-2** ($5{\cdot}10^{-6}$ M) in DMSO/H_2O mixtures. c) Denaturation study of **GluPc-2** (70% H_2O, $5{\cdot}10^{-6}$ M) monitored by absorption (left) and emission (center), and corresponding denaturation curves (right) plotting the spectral changes vs. the volume fraction of DMSO.

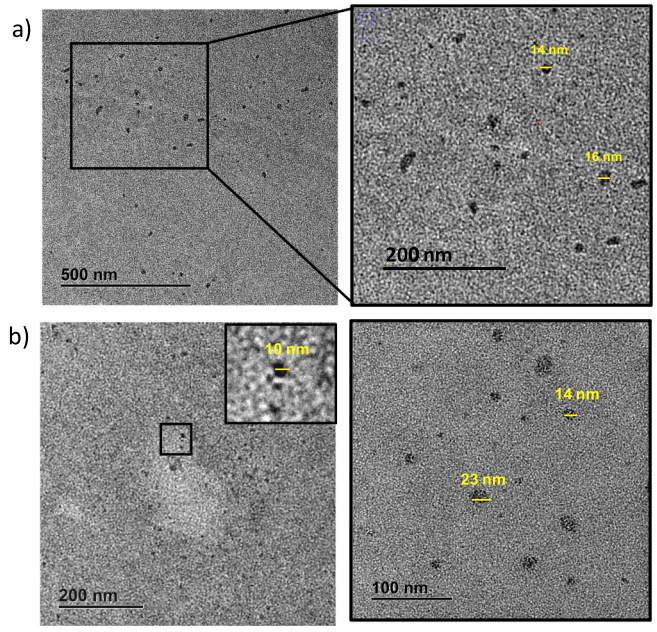

Fig. 4. TEM images of a) **GluPc-1** and b) **GluPc-2** prepared from water solutions (1% DMSO) at $8{\cdot}10^{-5}$ M concentration.

gradual dissociation through the stepwise addition of increasing volumes of the monomer solution in the good solvent (i.e., DMSO) over the aggregated species. The evolution of the system was monitored by UV–vis and fluorescence. As shown in Fig. 3c, two different equilibria were identified clearly in the UV–vis spectrum. Between 70% and 35% water content, the red-shifted band at 796 nm progressively disappeared, suggesting the disruption of the *J*-type aggregate. From 35% water onwards, the system transitioned directly towards the monomeric form. The changes in the Q-band intensity correlated well with fluorescence emission, with both techniques displaying two comparable sigmoidal transitions when plotted against the DMSO volume fraction. While the appearance of a red-shifted absorption band is promising for phototherapeutic applications, it is important to note that solutions containing 30% DMSO are unsuitable for biological experiments, due to the cytotoxicity of the solvent at such concentrations. Therefore, we attempted to obtain the same *J*-aggregated species in 99% H_2O solutions, considering the possibility that the initially observed *H*-aggregate could be a kinetically trapped species under these high-water-content conditions (99%), as there was no evolution in the UV spectra of the solution over time (see Fig. S5). It was reasoned that this kinetic aggregate might transition into a more thermodynamically stable *J*-aggregate upon application of an external stimulus, such as increased temperature. However, heating the solution up to 95 °C did not induce any spectral changes; instead, precipitation of the compound was observed. This suggests that the energy barrier between the kinetic *H*-aggregate and a more stable reorganized aggregate is quite high, and likely increases with the water content.

The aggregates were also characterized by CD spectroscopy, as the presence of the binaphthol unit is expected to generate CD signals. CD spectra of both derivatives were first recorded at $2{\cdot}10^{-5}$ M concentration in pure DMSO and water/DMSO 90:10 solutions. Distinct CD profiles were observed for the monomeric species in DMSO and their corresponding aggregates in aqueous media (see Fig. S6). In DMSO solutions, low intense CD signals are observed in the Soret band region, and almost negligible in the Q-band region. In 90% H_2O solutions, there is a change in the CD signal of both regions, that is, the evolution of bisignated bands with crossover in the wavelength of the absorption maxima in the UV–vis spectra of the aggregated species, which can be attributed to the formation of chiral aggregates. When studying **GluPc-2** solutions at 70% H_2O, a new crossover was observed around 800 nm, which correlates with the new red-shifted band observed in the UV–vis spectra at the same conditions.

To elucidate the size and shape of the aggregates, **GluPc-1** and **GluPc-2** solutions were analysed by TEM (see Fig. 4). Both **GluPc-1** and **GluPc-2** formed similar NPs, exhibiting amorphous shapes with

diameters ranging 15–30 nm. Additionally, DLS measurements were performed on freshly prepared $3{\cdot}10^{-6}$ M solutions in H_2O (1% DMSO), indicating average aggregate sizes of 26 ± 9 nm for **GluPc-1** and 21 ± 5 nm for **GluPc-2** (see Fig. S7 and S8). Comparable NP sizes were observed after 6 h incubation, indicating colloidal stability over time. The small NP sizes observed may be rationalized from the molecular structure of the compounds, which hold binaphthol units that are almost perpendicular to the Pc core (see Fig. S9). Consequently, in the initial stages of aggregation, the Pc cores can accommodate in a cofacial manner but rotating through the axial Pc axis, preventing the naphthol units from overlapping. However, further growing of aggregates is probably restricted by the steric hinderance originated by the binaphthol units.

Finally, the stability of the NPs in the culture medium used for the in vitro experiments (see below) was evaluated by UV–vis spectroscopy. The molar extinction coefficients of **GluPc-1** and **GluPc-2** main absorption bands did not change during the first 8 h (Fig. S10). This finding indicates that the NPs maintain their integrity over this period, and that the Pc components remain stable throughout the maximum incubation time used in the biological experiments (see below). After this initial period, the NP solutions were exposed to red-light LED irradiation for an additional 52 h, to assess their long-term photo- and colloidal stability. The formation of a precipitate could be observed for both samples, likely resulting from NP agglomeration (Fig. S11a-d), which produced an overall decrease in the absorption. However, after manually shaking the cuvette, the precipitate re-dissolved, and the absorption profiles nearly returned to those of freshly prepared solutions (Fig. S11e and S11f). These results indicate that the Pc components are photostable and that the chromophores remain embedded in the NP structure in the culture medium. Importantly, at no point during the experiment was an increase observed in the absorption band corresponding to the monomeric Pc species, suggesting that the NPs remained intact during the cell incubation.

2.3. Biological studies

To examine the targeting effect of the glucose moieties in **GluPc-1** and **GluPc-2**, the cellular uptake of these NPs was studied using the GLUT1-positive HT29 human colorectal adenocarcinoma cells and A549 human lung carcinoma cells, as well as the non-cancerous human embryonic kidney cells HEK293 used as the negative control. These cells were incubated with **GluPc-1** and **GluPc-2** (5 μM) for 2, 4, and 8 h, respectively, and then examined using confocal fluorescence microscopy. As shown in Fig. 5a and b, bright red fluorescence from the Pcs was observed inside all cells. This observation demonstrates the presence of photophysically active Pc units, consistent with either the release of fluorescent monomeric species or a NP rearrangement within the cellular microenvironment that triggers a fluorescent response upon internalization. After 2 h incubation, the red fluorescence was bright in A549 cells, a bit weaker in HT29 cells, but much weaker in HEK293 cells. The fluorescence intensity increased slightly upon prolonged incubation (to 4 and 8 h) for all the three cell lines. As shown in the summarized data in Fig. 5c and d, the intracellular fluorescence intensities of both Pcs in A549 cells were up to 3-fold higher than those in HEK293 cells, particularly for short-term incubation (2 and 4 h), with somewhat larger intensity differences for **GluPc-1** than for **GluPc-2**. A plausible explanation for the slightly higher uptake of **GluPc-1** is the larger size of its NPs, which would result in a greater number of Pc units being delivered to the cells. Another possible contributing factor is a lower degree of disassembly of **GluPc-2**, which could lead to reduced fluorescence intensity.

To determine whether GLUT1 is involved in the higher uptake of the Pc NPs by HT29 and A549 cells, a competition assay was performed using free glucose as a competitor. During the incubation of the cells with the Pc NPs (5 μM) for 4 h, glucose was added at concentrations ranging from 2 mM (400 equiv) to 10 mM (2000 equiv) for co-incubation. Confocal microscopy was again employed to analyze the

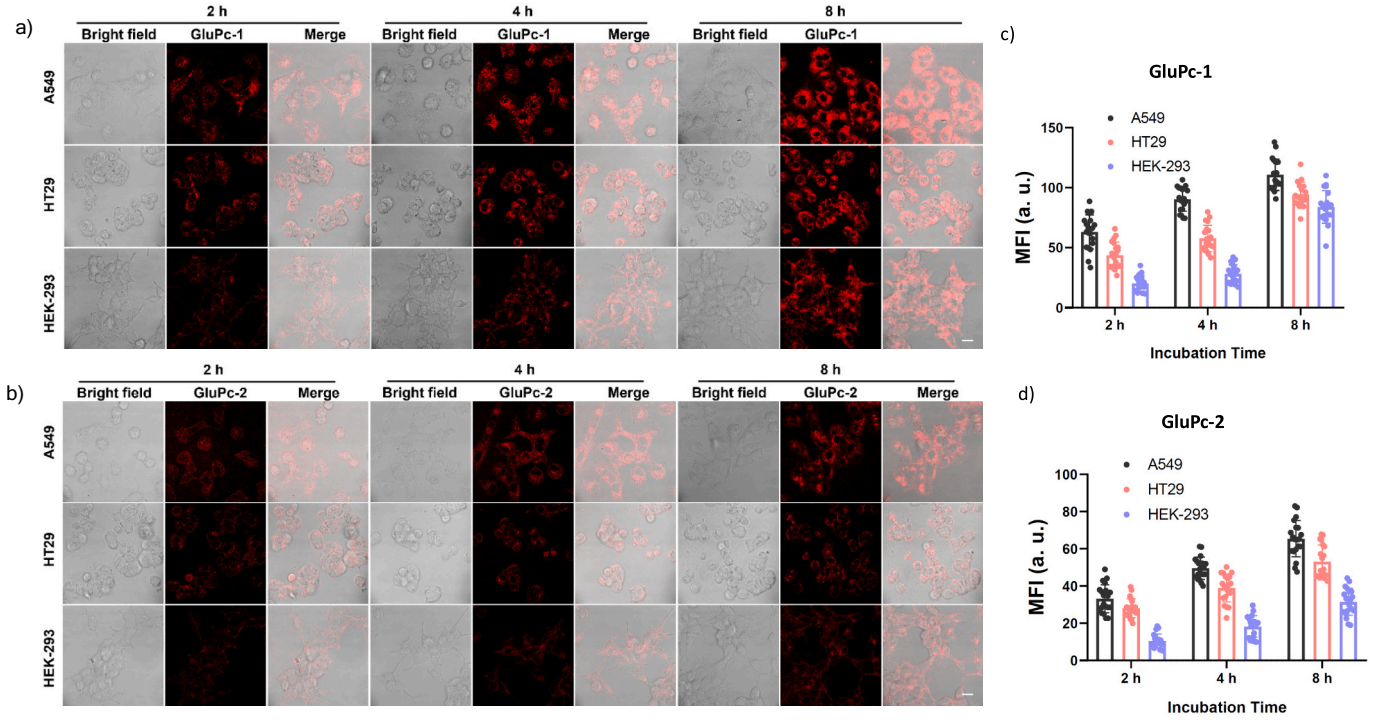

Fig. 5. Confocal images of A549, HT29 and HEK-293 cells after incubation with a) **GluPc-1** NPs and b) **GluPc-2** NPs at 5 μM concentration for 2, 4, and 8 h. The excitation and emission wavelengths used were 638 and 680–780 nm respectively (scale bar = 20 μm). Mean fluorescence intensities of different cells after incubation with c) **GluPc-1** NPs and d) **GluPc-2** NPs at 5 μM concentration for 2, 4, and 8 h recorded using confocal microscopy (λ_{exc} = 638 nm, λ_{em} = 680–780 nm). Data are expressed as the mean ± standard deviation (SD) of twenty cells.

intracellular fluorescence intensity. As shown in Figs. S12 and S13, intracellular fluorescence was significantly reduced in the presence of glucose, with the intensity decreasing in a concentration-dependent manner in both cell lines. These results suggest that the uptake of Pcs or Pc NPs by cancer cells is competitively inhibited by glucose, indicating the involvement of GLUT1.

The cytotoxicity of Pc NPs against HT29, A549, and HEK293 cells was then evaluated using the MTT assay. Fig. 6 shows the dose-dependent survival curves of **GluPc-1** and **GluPc-2** for the three cell lines, both in the absence or presence of light irradiation ($\lambda > 610$ nm, 40 mW cm^{-2}, 48 J·cm^{-2}). Treatment with the **GluPc-1** and **GluPc-2** NPs resulted in negligible dark toxicity up to Pc concentrations of 5 μM. Upon light irradiation, the cytotoxicity was increased for the three cell lines due to the PDT effect of the Pc moieties. The half maximal inhibitory concentrations (IC_{50}) of **GluPc-1** NPs were determined for each cell line (Table 2). GLUT1-positive A549 exhibited the lowest IC_{50} value (0.55 μM). In contrast, higher IC_{50} values were obtained for HT29 (0.89 μM) and for the GLUT1-negative control HEK293 (1.10 μM). Accordingly, the selectivity index (SI) of **GluPc-1** between A549 and HEK293 cells was 2.0, whereas the SI between HT29 and HEK293 cells was lower (1.2). This difference is likely associated with variations in glucose transporter and glycan expression among the cell lines. Previous studies have reported high GLUT1 expression in A549 cells and comparatively lower levels in HT29 cells, which may account for the observed differences in uptake and cytotoxic selectivity [24,25]. For **GluPc-2** NPs slightly lower IC_{50} values were obtained overall: 0.50 μM for A549, and 0.74 and 0.89 μM for HT29 and HEK293 cells, respectively. Consistent with the previous trend, the SI of **GluPc-2** was higher between A549 and HEK293 cells (1.78) than between HT29 and HEK293 cells (1.2).

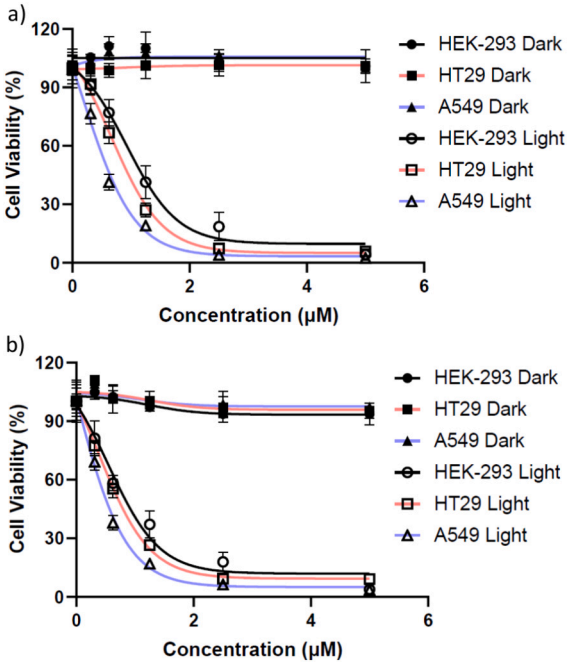

Fig. 6. Cytotoxic effect of a) **GluPc-1** and b) **GluPc-2** against A549, HT29 and HEK293 cells in the absence and presence of light (20 min irradiation, $\lambda > 610$ nm, 40 mW cm^{-2}, 48 J·cm^{-2}), incubated for 4 h.

Table 2
IC_{50} values (in μM) of **GluPc-1** and **GluPc-2** in different cell lines.

Compound	A549	HT29	HEK293
GluPc-1	0.55	0.89	1.10
GluPc-2	0.50	0.74	0.89

3. Conclusion

In this study, two amphiphilic AABB-type Zn(*II*)Pcs functionalized with glucose units (**GluPc-1** and **GluPc-2**) were designed to self-assemble in aqueous media, aiming to generate NPs with enhanced tumor-targeting and improved PDT performance. Both compounds were satisfactorily prepared from a dibromo-binaphthyloxy-linked AABB-Zn(*II*)Pc synthon, through a Sonogashira coupling or click chemistry protocol. As expected, the UV–vis and fluorescence spectra of **GluPc-1** and **GluPc-2** in water:DMSO (99:1) exhibited characteristic signatures of aggregation. TEM and DLS analyses further confirmed the formation of well-defined NPs with good colloidal stability and diameters in the 15–30 nm range. Confocal microscopy studies over cells incubated with these NPs demonstrated: i) a recovery of the fluorescent properties which is relevant for PDT treatment; ii) a preferential internalization into cancer cell lines overexpressing GLUT1 (A549 and HT29), confirming that the glucose residues exposed on the NP surface mediate selective recognition by glucose transporters. Competition experiments with free glucose further validated GLUT1 involvement in this mechanism. Both compounds showed negligible dark toxicity but pronounced light-induced cytotoxicity, achieving sub-micromolar IC_{50} values, particularly against A549 cells. These results underscore the potential of self-assembled glycosylated Pcs as tumor-selective nanomaterials for PDT, combining high specificity with potent photodynamic efficacy. Overall, this work demonstrates that the self-assembly of amphiphilic PS bearing recognition motifs provides an effective strategy to engineer next-generation functional NPs with strong promise for cancer therapy.

4. Experimental section

4.1. General methods and characterization techniques

All chemical reagents and solvents were analytical grade and were used without further purification. All reactions were performed in standard glassware, except for the cyclotetramerization reactions that were carried out in high pressure sealed tubes. Analytical TLC was carried out employing aluminium sheets coated with silica gel type 60 F254 (0.2 mm thick, E. Merck). Purification and separation of the synthesized products was performed by column chromatography, using silica gel (230–400 mesh, 0.040–0.063 mm, Merck). Eluents and relative proportions of the solvents are indicated for each particular case. Size exclusion chromatography was performed using Bio-Beads S-X1 (200–400 mesh, Bio-Rad). Anion exchange was performed using Dowex® resin. Mass Spectrometry (MS) and High-Resolution Mass Spectrometry (HRMS) spectra were recorded employing Electrospray Ionization (ESI Positive TOF_MS) mass spectra using an API Q-Star Pulsar i from Sciex, or Matrix Assisted Laser Desorption/Ionization-Time of Flight (MALDI-TOF) using a Bruker Ultraflex III TOF/TOF spectrometer, with a nitrogen laser operating at 337 nm, or with a NdYAG laser operating at 335 nm. The different matrixes employed are indicated for each spectrum. Mass spectrometry data are expressed in *m/z* units. All MS experiments were carried out at the Servicio Interdepartmental de Investigación (SIdI) of the Universidad Autónoma de Madrid. ^{1}H NMR and ^{13}C NMR were recorded on Bruker XRD-300 (300 MHz) and XRD-500 (500 MHz) instruments. Deuterated solvents employed are indicated in each spectrum.

4.2. Synthesis

The synthesis of Zn(*II*)Pc precursors **AABB-Br** [10], **AABB-alk** [12] and **AABB-alkH** [12] was performed following reported procedures. Compounds **AA-Br** [10], **Glu-1** and **Glu-2** [18] were also synthesized as described in literature.

4.2.1. Preparation of *AA-Glu*

$Pd(PPh_3)_4$ (33.2 mg, 0.029 mmol), **Glu-1** (138.7 mg, 0.359 mmol)

and **AA-Br** (100 mg, 0.144 mmol) were added to a Schlenk flask. The mixture was dissolved in dry DMF (1.38 mL) and freshly distilled Et_3N (1.38 mL) at room temperature. The reaction mixture was then heated at 80 °C under argon atmosphere and maintained under continuous stirring for 3 h. Solvents were removed under reduced pressure obtaining a brown oil. Purification was carried out by flash column chromatography (heptane/EtOAc 1:2) obtaining **AA-Glu** (157 mg) as a yellow solid in 84% yield. ^{1}H NMR (300 MHz, DMSO-d_6): δ 8.28 (s, 2H, H_{Ar}), 8.23 (d^3, J = 9.1 Hz, 2H, H_{Ar}), 7.68 (d^3, J = 8.1 Hz, 2H, H_{Ar}), 7.64–7.57 (m, 4H, H_{Ar}), 7.39 (d^3, J = 9.1 Hz, 2H, H_{Ar}), 7.31 (d^3, J = 8.4 Hz, 2H, H_{Ar}), 7.26 (d^3, J = 8.4 Hz, 2H, H_{Ar}), 5.34 (t^3, J = 9.6 Hz, 2H, O—CH), 5.04 (d^3, J = 8.0 Hz, 2H, O—CH), 4.94 (t^3, J = 9.6 Hz, 2H, O—CH), 4.82 (dd^3, J = 9.6 Hz^3, J = 8.0 Hz, 2H, O—CH), 4.67 (d^3, J = 15.6 Hz, 2H, O—CH_2—C_{sp}), 4.56 (d^2, J = 15.6 Hz, 2H, O—CH_2—C_{sp}), 4.26–4.15 (m, 2H, O—CH), 4.06–4.00 (m, 4H, AcO—CH_2), 1.99 (s, 18H, OAc), 1.94 (s, 6H, OAc) ppm. ^{13}C NMR (76 MHz, DMSO-d_6): δ; 170.1 (C), 169.6 (C), 169.3 (C), 169.1 (C), 158.9 (C), 150.5 (C), 135.7, 132.5, 132.0, 131.5, 130.7, 129.7, 128.2, 125.7, 122.0, 121.6, 120.7, 119.3, 115.6, 115.4, 112.6, 104.6 (CH), 98.1, 86.0, 85.8, 72.1, 70.9, 70.7, 68.1, 61.7, 56.4, 20.5 (CH_3), 20.4 (CH_3), 20.3 (CH_3) ppm. HR-MS (ESI Positive): Calculated for $C_{70}H_{58}O_{22}N_4Na$ [M + Na]$^+$: 1329.3435; Found [M + Na]$^+$: 1329.3418; Calculated for $C_{70}H_{58}O_{22}N_4Na_2$ [M + 2Na]$^{2+}$: 676.1664; Found [M + 2Na]$^{2+}$: 676.1658.$[\alpha]_D^{20}$ = +50.8° (c = 0.4, CH_2Cl_2).

4.2.2. Preparation of *GluAABB-1*

Method 1: $Pd(PPh_3)_4$ (3.3 mg, 0.003 mmol), **Glu-1** (14 mg, 0.036 mmol) and **AABB-Br** (15 mg, 0.014 mmol) were added to a Schlenk flask. The mixture was dissolved in anhydrous DMF (0.47 mL) and freshly distilled Et_3N (0.2 mL). The reaction mixture was heated at 80 °C under argon atmosphere and maintained under continuous stirring for 2 h. Solvents were removed under reduced pressure obtaining a blue solid. Purification was carried out by flash column chromatography (heptane/THF 1:1). The fraction containing the product was further purified by a second flash column chromatography (heptane/THF 2:1). The product was washed with MeOH, obtaining **GluAABB-1** (8 mg) as a blue solid in 34% yield. Method 2: Bisphthalonitrile **AA-Glu** (78.2 mg, 0.060 mmol), phthalonitrile (15.3 mg, 0.120 mmol) and anhydrous $Zn(AcO)_2$ (16.5 mg, 0.090 mmol) were placed in a high-pressure resistant flask equipped with a magnetic stirrer, and then dry *o*-DCB/DMF (dried over 4 Å molecular sieves) 2:1 were added, for [**AA-Glu**] = 0.05 M. The mixture was heated to 150 °C overnight under argon atmosphere. After cooling, the solvent was removed under reduced pressure. The blue solid was filtered in a silica gel plug with THF. After evaporation of the solvent, the product was purified by size exclusion chromatography on Bio-Beads using THF as eluent, monitored by TLC (heptane/THF, 1:2, 1% pyridine), obtaining pure **GluAABB-1** as a blue solid (9.7 mg) in 10% yield. ^{1}H NMR (300 MHz, DMSO-d_6): δ_H; 8.85 (d^3, J = 7.3 Hz, 2H, H_{Ar}), 8.74 (d^3, J = 6.6 Hz, 2H, H_{Ar}), 8.46 (d^3, J = 6.6 Hz, 2H, H_{Ar}), 8.29 (s, 2H, H_{Ar}), 8.26 (d^3, J = 9.4 Hz, 2H, H_{Ar}), 8.05–7.96 (m, 2H, H_{Ar}), 7.95–7.88 (m, 4H, H_{Ar}), 7.85–7.68 (m, (H, H_{Ar}), 5.34 (t^3, J = 9.6 Hz, 2H, O—CH), 5.07 (d^3, J = 8.0 Hz, 2H, O—CH), 4.94 (t^3, J = 9.6 Hz, 2H, O—CH) 4.83 (dd^3, J = 9.6 Hz^3, J = 8.0 Hz, 2H, O—CH), 4.68 (d^2, J = 18.0 Hz, 2H, O—CH_2—C_{sp}), 4.57 (d^2, J = 18.0 Hz, 2H, O—CH_2—C_{sp}), 4.23–4.16 (m, 2H, O—CH), 4.11–4.01 (m, 4H, AcO—CH_2), 2.00 (s, 12H, OAc), 1.96 (s, 6H, OAc), 1.92 (s, 6H, OAc) ppm. ^{13}C NMR (126 MHz, DMSO) δ 170.1 (C), 169.6 (C), 169.3 (C), 169.1 (C), 155.8, 152.5, 152.0, 150.9, 149.5, 148.5, 140.8, 137.1, 136.9, 134.1, 132.1, 130.0, 129.1, 128.9, 125.5, 121.8, 120.3, 118.4, 116.9, 114.6, 97.9 (CH), 86.6 (C), 84.9 (C), 72.1, 70.9, 70.7, 68.1, 61.7, 56.7 (CH_2), 20.5 (CH_3), 20.5 (CH_3), 20.4 (CH_3), 20.3 (CH_3). HR-MS (MALDI, matrix DCTB + PPGNa 1000 + PPGNa 2000): calculated for $C_{86}H_{66}N_8O_{22}Zn$ [M]$^+$: 1626.3583; Found [M]$^+$: 1626.3578. UV–vis (DMSO) log(ε/M^{-1} cm^{-1}) (λ): 5.1 (348 nm); 5.8 (680 nm). Fluorescence: $\lambda_{maximum}$ = 688 nm; $\lambda_{excitation}$ = 650 nm.

4.2.3. Preparation of *GluPc-1*

GluAABB-1 (7.6 mg, 0.005 mmol) was dissolved in 0.3 mL DMSO and added over a prepared solution of Na (0.34 mg, 0.015 mmol) in dry MeOH (0.1 mL). The reaction mixture was stirred at r.t. overnight. Then, ion exchange resin Amberlite IR-120H (20 mg) was added to neutralize the solution. The solution was filtered to remove the resins. The MeOH is evaporated under reduced pressure. The product is precipitated from the DMSO solution by addition of milliQ water (6 mL. The solid is filtered and washed with H_2O and the MeOH for several times. **GluPc-1** was obtained as a blue solid in 97% yield (6 mg). ^{1}H NMR (300 MHz, DMSO-d_6) δ 8.94 (d^3, J = 6.8 Hz, 2H, H_{Ar}) 8.92–8.85 (m, 2H, H_{Ar}), 8.71–8.62 (m, 2H, H_{Ar}), 8.25 (s, 2H, H_{Ar}), 8.21 (d^3, J = 9.1 Hz, 2H, H_{Ar}), 8.06 (t^3, J = 7.4 Hz, 2H, H_{Ar}), 8.00–7.82 (m, 8H, H_{Ar}), 7.74 (d^3, J = 8.7 Hz, 2H, H_{Ar}), 7.68 (d^3, J = 9.1 Hz, 2H, H_{Ar}), 5.10 (d^3, J = 4.9 Hz, 2H, —OH), 4.72 (d^2, J = 15.8 Hz, 2H, O—CH_2—C_{sp}), 4.58 (d^2, J = 15.8 Hz, 2H, O—CH_2—C_{sp}), 4.52 (t^3, J = 4.9 Hz, 2H, —OH), 4.35 (d^3, J = 7.7 Hz, 2H, O—CH), 3.74–3.63 (m, 2H, O—CH), 3.50–3.40 (m, 2H, O—CH), 3.19–3.09 (m, 2H, O—CH), 3.08–2.96 (m, 2H, O—CH) ppm.^{13}C NMR (500 MHz, DMSO-d_6, 343 K) δ 155.4, 151.4, 149.6, 148.48, 140.6, 133.8, 131.5, 130.0, 129.6, 129.0, 128.6, 125.0, 124.6, 122.0, 121.8, 119.9, 117.0, 114.0, 101.0 (CH), 85.7 (C), 85.6 (C), 76.7, 76.6, 73.1, 70.1, 61.1, 55.6 (CH_2) ppm. HR-MS (MALDI, matrix Ditranol + NaI): calculated for $C_{70}H_{50}N_8O_{14}Zn$ [M]$^+$: 1290.2738; Found [M]$^+$: 1290.2732. UV–vis (DMSO): log(ε/M^{-1} cm^{-1}) (λ): 4.7 (350 nm); 4.4 (612 nm); 5.2 (680 nm). Fluorescence (DMSO): $\lambda_{maximum}$ = 687 nm; $\lambda_{excitation}$ = 650 nm.

4.2.4. Preparation of *GluAABB-2*

AABB-alkH (48 mg, 0.053 mmol) was dissolved in dry THF (8 mL) under Ar atmosphere. Then, sequentially are added a solution of $CuSO_4{\cdot}5H_2O$ (13.2 mg, 0.053 mmol) in 1 mL H_2O, a solution **Glu-2** (55 mg, 0.132 mmol) in 4 mL of THF/H_2O 3:1, and finally, a solution of sodium ascorbate (40.5 mg, 0.053 mmol) in 1 mL H_2O. The reaction was stirred overnight at rt. After that, the crude was treated with Quadrasil MP, filtered, and evaporated. The product was dissolved in THF (2 mL) and precipitates upon addition of MeOH (15 mL). The solid obtained is filtered and washed with H_2O and MeOH several times. The product was obtained as a blue solid in 60% yield (55 mg). ^{1}H NMR (300 MHz, DMSO-d_6) δ 9.14–8.97 (m, 4H, H_{Ar}), 8.90–8.78 (m, 2H, H_{Ar}), 8.57–8.49 (m, 4H, H_{Ar}), 8.26–8.09 (m, 6H, H_{Ar}), 8.05–7.92 (m, 6H, H_{Ar}), 7.70 (d^3, J = 8.7 Hz, 2H, H_{Ar}), 5.21 (t^3, J = 9.5 Hz, 2H, O—CH), 4.94–4.80 (m, 4H, O—CH), 4.78–4.71 (m, 2H, O—CH), 4.68–4.54 (m, 4H, O—CH), 4.22–4.13 (m, 4H, O—CH, —CH_2), 4.05–3.93 (m, 6H, —CH_2), 1.98 (s, 6H, OAc), 1.94 (s, 6H, OAc) 1.89 (s, 6H, OAc), 1.77 (s, 6H, OAc) ppm.^{13}C NMR (300 MHz, DMSO-d_6) δ170.1 (C), 169.6 (C), 169.3 (C), 169.0 (C), 155.2, 151.8, 150.8, 149.6, 149.6, 148.8, 146.4, 140.9, 137.0, 136.8, 134.2, 130.0, 129.3, 126.4, 121.9, 121.7, 120.2, 118.8, 99.3 (CH), 71.9, 70.7, 68.1, 49.5, 20.4 (CH_3), 20.4 (CH_3), 20.2 (CH_3), 20.2 (CH_3) ppm. HR-MS (MALDI, matrix DCTB+ PEGNa 1500): calculated for $C_{88}H_{72}N_{14}O_{22}Zn$ [M]$^+$: 1740.4245; Found [M]$^+$: 1740.4270. UV–vis (DMSO): log(ε/M^{-1} cm^{-1}) (λ): 4.3 (344 nm); 4.0 (613 nm); 4.7 (680 nm). Fluorescence (DMSO): $\lambda_{maximum}$ = 685 nm; $\lambda_{excitation}$ = 650 nm.

4.2.5. Preparation of *GluPc-2*

GluAABB-2 (48 mg) was dissolved in DMSO (1.1 mL) and added over a prepared solution of Na (2 mg, 0.087 mmol) in dry MeOH (0.53 mL). The reaction mixture was stirred at r.t. overnight. Then, ion exchange resin Amberlite IR-120H (20 mg) was added to neutralize the solution. The solution was filtered to remove the resins. The MeOH is evaporated under reduced pressure. The product is precipitated from the DMSO solution by addition of milliQ water (6 mL. The solid is filtered and washed with H_2O and the MeOH for several times. **GluPc-2** was obtained as a blue solid in 98% yield (38 mg). ^{1}H NMR (300 MHz, DMSO-d_6) δ 9.12–8.86 (m, 4H, H_{Ar}), 8.78 (s, 2H, H_{Ar}), 8.88–8.65 (m, 2H, H_{Ar}), 8.53 (s, 2H, H_{Ar}), 8.27–8.20 (m, 2H, H_{Ar}), 8.18–8.07 (m, 4H, H_{Ar}), 8.04–7.86 (m, 8H, H_{Ar}), 7.78–7.66 (m, 2H, H_{Ar}), 5.24 (s, 2H, —OH), 4.96

(s, 2H, —OH), 4.91 (s, 2H, —OH), 4.77–7.60 (m, 4H, O—CH_2), 4.52 (s, 2H, —OH), 4.30 (d^3, J = 8.7 Hz, 2H, O—CH), 4.23–4.12 (m, 2H, —CH_2—), 4.03–4.90 (m, 2H, —CH_2—), 3.76–3.70 (m, 2H, HO—CH_2—), 3.53–3.47 (m, 2H, HO—CH_2—), 3.20–3.10 (m, 4H, O—CH), 3.08–2.97 (m, 4H, O—CH) ppm. ^{13}C NMR (500 MHz, DMSO-d_6, 343 K) δ 154.6, 146.1, 133.8, 129.4, 129.2, 126.3, 123.8, 121.8, 118.4, 102.6 (CH), 76.5 (CH), 73.1 (CH), 70.0 (CH), 66.8 (CH_2), 61.0 (CH_2), 49.5 (CH_2) ppm. HR-MS (MALDI, matrix DCTB + ACC): calculated for $C_{72}H_{57}N_{14}O_{14}Zn$ $[M + H]^+$: 1407.3469; Found $[M + H]^+$: 1407.3430. UV–vis (DMSO): $\log(\varepsilon/M^{-1}\ cm^{-1})$ (λ): 4.7 (351 nm); 4.5 (613 nm); 5.3 (680 nm). Fluorescence (DMSO): $\lambda_{maximum}$ = 688 nm; $\lambda_{excitation}$ = 650 nm.

CRediT authorship contribution statement

Irene Paramio: Writing – original draft, Methodology, Investigation, Formal analysis, Data curation. **Gaole Dai:** Writing – review & editing, Methodology, Investigation, Formal analysis, Data curation. **Tomás Torres:** Visualization, Project administration. **Dennis K.P. Ng:** Writing – review & editing, Validation, Supervision. **Gema de la Torre:** Writing – review & editing, Writing – original draft, Validation, Supervision, Resources, Project administration, Funding acquisition, Formal analysis, Conceptualization.

Declaration of competing interest

The authors declare that they have no known competing financial interests or personal relationships that could have appeared to influence the work reported in this paper.

Acknowledgements

This work has been supported by the Spanish MICIU/AEI/10.13039/501100011033/FEDER, UE (PID2023-149483NB-C21, PID2023-151167NB-I00), the Comunidad de Madrid and the Spanish State through the Recovery, Transformation and Resilience Plan ["Materiales Disruptivos Bidimensionales (2D)" (MAD2D-CM) (UAM1)-MRR Materiales Avanzados], and the European Union through the Next Generation EU funds. IMDEA Nanociencia acknowledges support from the "Severo Ochoa" Programme for Centres of Excellence in R&D (MINECO, CEX2020-001039-S). This work was also financially supported by the Research Grants Council of the Hong Kong Special Administration Region, China, through the Collaborative Research Fund (Ref. No. C4057-24GF).

Appendix A. Supplementary data

Supplementary data to this article can be found online at https://doi.org/10.1016/j.bioorg.2025.109376.

Data availability

Data will be made available on request.

References

[1] D.E.J.G.J. Dolmans, D. Fukumura, R.K. Jain, Nat. Rev. Cancer 3 (2003) 380–387, https://doi.org/10.1038/nrc1071.
[2] K. Plaetzer, B. Krammer, J. Berlanda, F. Berr, T. Kiesslich, Lasers Med. Sci. 24 (2009) 259–268.
[3] H. Maeda, J. Wu, T. Sawa, Y. Matsumura, K. Hori, J. Control. Release 65 (2000) 271–284.
[4] X. Li, S. Lee, J. Yoon, Chem. Soc. Rev. 47 (2000) 1174–1188.
[5] I. Paramio, T. Torres, G. de la Torre, ChemMedChem 16 (2021) 2441–2451.
[6] L. Zhao, Y. Xing, R. Wang, F.F. Yu, F. Yu, ACS Appl. Bio Mater. 3 (2020) 86–106.
[7] P.C. Lo, M.S. Rodríguez-Morgade, R.K. Pandey, D.K.P. Ng, T. Torres, F. Dumoulin, Chem. Soc. Rev. 49 (2020) 1041–1056.
[8] A. Galstyan, Chem. Eur. J. 27 (2021) 1903–1920.
[9] N.J. Hestand, F.C. Spano, Chem. Rev. 118 (2018) 7069–7163.
[10] M.A. Revuelta-Maza, T. Torres, G. de la Torre, Org. Lett. 21 (2019) 8183–8186.
[11] K. Nolan, M. Hu, C. Leznoff, Synlett (1997) 593–594.
[12] T. Fukuda, N. Kobayashi, Chem. Lett. 31 (2002) 866–867.
[13] H. Miwa, N. Kobayashi, Chem. Lett. 28 (1999) 1303–1304.
[14] N. Kobayashi, H. Miwa, V.N. Nemykin, J. Am. Chem. Soc. 124 (2002) 8007–8020.
[15] M.A. Revuelta-Maza, E. de las Heras, M. Agut, S. Nonell, T. Torres, G. de la Torre, Chem. Eur. J. 27 (2021) 4955–4963.
[16] I. Paramio, A. Salazar, M. Jordà-Redondo, S. Nonell, T. Torres, G. de la Torre, Adv. Ther. 6 (2023) 2300116.
[17] I. Paramio, T. Torres, G. de la Torre, Org. Chem. Front. 11 (2023) 60–66.
[18] S. Park, I. Shin, Org. Lett. 9 (2007) 1675–1678.
[19] J. Pan, A. Ouyang, W. Fang, G. Cheng, W. Liu, F. Wang, D. Zhao, K. Le, J. Jiang, J. Mater. Chem. B 8 (2020) 2895–2908.
[20] F. Tang, H. Yu, Y. Huang, X. Zhao, Z. Chen, H. Ma, B.-Y. Zheng, M.-R. Ke, Y. Zhang, X. Li, J. Yoon, J.-D. Huang, Chem. Eng. J. 496 (2024) 154272.
[21] E. Yabas, M. Sülü, S. Saydam, F. Dumludag, B. Salih, O. Bekaroglu, Inorg. Chim. Acta 365 (2011) 340–348.
[22] K. Kameyama, M. Morisue, A. Satake, Y. Kobuke, Angew. Chem. Int. Ed. 44 (2005) 4763–4766.
[23] F. Bächle, C. Maichle-Mössmer, T. Ziegler, ChemPlusChem 84 (2019) 1829–1836.
[24] H. Zhao, J. Sun, J. Shao, Z. Zou, X. Qiu, E. Wang, G. Wu, J. Cancer 10 (2019) 4989–4997.
[25] S. Hauptmann, V. Grünewald, D. Molls, W.D. Schmitt, M. Köbel, K. Kriese, A. Schürmann, Anticancer Res. 25 (2005) 3431–3436.